Selenium adsorption on Mo(110): A first-principles investigation

Guido Roma[1,2] and Letizia Chiodo[3,*]

[1]*CEA, DEN, Service de Recherche de Métallurgie Physique, F-91191 Gif-sur-Yvette, France*

[2]*Institut für Anorganische Chemie und Analytische Chemie, Johannes Gutenberg Universität, D-55128 Mainz, Germany*

[3]*Center for Biomolecular Nanotechnologies @UNILE, Istituto Italiano di Tecnologia, and European Theoretical Spectroscopy Facility (ETSF), Via Barsanti, I-73010 Arnesano, Italy*

(Received 8 January 2013; revised manuscript received 6 May 2013; published 17 June 2013)

Selenium adsorption on molybdenum surfaces is a relevant process in the production of thin-film solar cells, in particular as far as the formation of the layered compound $MoSe_2$ is concerned. In this paper we investigate the energetics of Se adsorption on the (110) surface of molybdenum using first-principles calculations in the two limiting cases of low and high coverage, and we establish a comparison with the more extensively investigated case of sulfur adsorption at submonolayer coverage. The studied system provides the opportunity for testing the most crucial approximations, namely, the choice of the exchange-correlation functional and the pseudopotential generation. We find that semicore states of molybdenum have an influence on calculated surface energies and, to a lesser extent, on adsorption energies. We compare some more or less popular semilocal exchange-correlation functionals, including one recently proposed as an improvement for quasi-two-dimensional systems. The results show that the preferred adsorption site changes with coverage and suggest a strong variation of the adsorption energy with coverage.

DOI: 10.1103/PhysRevB.87.245420 PACS number(s): 68.43.Bc, 68.43.Fg, 68.35.Md

I. INTRODUCTION

Thin-film photovoltaics technology exploits the high absorbance properties of materials, in particular of copper indium gallium selenide ($CuIn_xGa_{1-x}Se_2$, CIGSe), to build thin-layered devices with efficiencies around 20%.[1,2] In such devices, one thing that must be done to improve performance is to reduce the losses occurring at the interfaces of the multilayered structure. Among the various interfaces, we focus here on the one between the quaternary chalcopyrite semiconductor and the metallic back contact, usually Mo; this interface also reflects the unabsorbed photons back into the CIGSe. When CIGSe is grown on the metal, the deposition of selenium leads to the formation of a $MoSe_2$ layer, whose presence is necessary as it lowers the Schottky barrier of the Mo/CIGSe interface, making the contact Ohmic.[3] The formation process of this layered compound is not well understood, whatever deposition procedure is employed. In order to gain a deeper understanding of the formation of $MoSe_2$ and of the interfacial properties of the Mo/$MoSe_2$/CIGSe structure, it would be helpful to know the basic features of Se adsorption on the relevant Mo surfaces; this knowledge could suggest alternative deposition procedures and/or allow for a better control of the final morphology.

Scarce and sparse data are available for this interface of basic technological interest.[4–7] Surprisingly enough, at variance with other adsorbates (O, S, Sb, Pd, Pb) for which computational studies of stability have been performed,[8–13] not much is known from theoretical approaches about the adsorption of Se on Mo surfaces.

Indeed, the surfaces of molybdenum have been a playground for benchmarking theoretical approaches to describe reconstructions, surface energies,[14] adsorption of several elements,[8–13] and peculiar vibrational effects.[15] Both fundamental interest and applied research issues have triggered these works. Oxygen and sulfur adsorption on Mo(110) have already been studied by first principles;[8,9,13] these studies were devoted to 0.5 and 0.25 monolayer (ML) coverage for sulfur—for this element a few specific adsorption structures could be compared with experimental STM images—and, additionally, to 1 ML coverage for oxygen, including some subsurface configurations.

In this paper we present a theoretical study, via density functional theory, of the adsorption of selenium at high and low coverage on the Mo (110) surface. The (110) is expected to be the lowest energy orientation[14] among Mo high-symmetry surfaces, and it should yield the highest efficiency[16] in CIGSe solar cells. We address the two limiting cases of adsorbed atoms: isolated from each other (0.11 ML) and full coverage (1 ML). We are not aware of specific patterns/coverages having been observed experimentally for the Se:Mo(110) system.

The paper is organized as follows. Section II describes the theoretical approach and technical details, in particular concerning the influence of pseudopotentials and of the exchange correlation (xc) functional. The results section (Sec. III) is subdivided into four subsections: the first (Sec. III A) is devoted to the results for molybdenum clean surfaces; the second, Sec. III B, presents Se on Mo(110) at 1 ML coverage; the third (Sec. III C) deals with intermediate coverages and adsorption structures, allowing a comparison with the case of sulfur adsorption; the fourth section (Sec. III D) reports on calculated adsorption energies at low coverage. The paper is concluded by Sec. IV, summarizing the main results and commenting on the differences among the considered functionals as far as Mo surface energies and Se adsorption on Mo(110) are concerned.

II. APPROACH AND TECHNICAL DETAILS

We performed first-principles calculations in the framework of density functional theory (DFT). We employed the plane waves pseudopotential approach as implemented in the QUANTUM-ESPRESSO package.[17] As surface energy and adsorption energy may be sensitive to the xc functionals,[18,19] we tested various semilocal approaches—some generalized gradient approaches (GGAs) and the local

density approximation (LDA)—to investigate this system for which experimental data are scarce or completely lacking.

In order to disentangle the effect of the functional from that of the pseudopotential approximation, we performed calculations with a few different pseudopotentials for each element. Some of them were generated by the authors by using the atomic code included in the QUANTUM-ESPRESSO package. We generated two sets of pseudopotentials for Se and Mo for five different functionals. One set of Mo pseudopotentials (pseudo set 1) includes only $4d$ and $5s$ channels as valence states, while the other (pseudo set 2) also contains semicore states $4s$ and $4p$. For a given element and pseudopotential set, the generation configuration (cutoff radii, electronic configuration) is kept the same for all functionals, allowing a fair comparison of different approximations for the xc term. All pseudopotential files are included as Supplemental Material for reproducibility.[20]

The functionals tested are LDA,[21] PBE,[22] PBEsol,[23] revPBE,[24] and the recently proposed Q2D-GGA.[19] Both PBEsol and revPBE are PBE variants; the former is optimized for solids and surfaces, while the latter improves atomization energies. Q2D-GGA outperforms other GGAs in cases of layered electronic charge, which are not unusual for transition metal surfaces. We also performed a few calculations with the hybrid functional HSE06,[25,26] for the sake of completeness. In this case, for both Mo and Se we used PBE norm-conserving pseudopotentials from a public library,[27] without semicore states. Hybrid functional calculations were performed with a kinetic energy cutoff of 40 Ry and a charge density cutoff of 160 Ry; the Fock exchange term was calculated on a grid of $3 \times 3 \times 3$ auxiliary $\mathbf{q}$ points for bulk Mo ($3 \times 3 \times 1$ for the surface slab) and the divergence at $\mathbf{q} = 0$ was treated with the Gygi-Baldereschi recipe[28] as implemented in the QUANTUM-ESPRESSO package.

For all Mo pseudopotentials the error is less than 1% on the lattice parameter and less than 10% on the bulk modulus; no clear difference between pseudopotentials with or without semicore states can be worked out for structural parameters. Nevertheless, by comparing the lattice parameter for different semilocal functionals, one can identify the following, expected trend: revPBE gives the largest lattice parameter, followed by PBE, PBEsol, and Q2D-GGA, while the LDA gives the lowest value. The reverse trend clearly holds for the bulk modulus. All calculated equilibrium lattice parameters and bulk moduli are compared to experimental data in Fig. 1; the best results with respect to experiments are obtained with LDA, Q2D-GGA, and PBEsol when semicore states are included.[29,30]

Considering selenium, the description of the structure of the trigonal bulk solid is extremely sensitive to the pseudopotential choice, and the error on the equilibrium volume can be quite large. Such a behavior is related to a very flat potential energy landscape associated with the peculiar structure of trigonal selenium and induced us to investigate this element in more detail. We checked the atomization energy of trigonal selenium, its formation energy with respect to the Se_2 molecule, and the binding energy of the latter; for all these quantities the maximum difference between distinct pseudopotentials amounts to 0.045 eV/atom, the worst case occurring with the revPBE functional. Moreover, checking a number of pseudopotentials (both homemade and from public libraries) on the solid

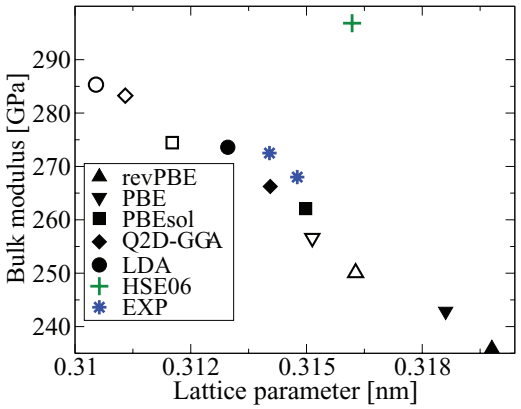

FIG. 1. (Color online) Lattice parameters and bulk moduli for Mo compared to experimental results. Solid symbols are for the pseudopotentials including $4s$-$4p$ semicore states in valence, while empty ones are for the pseudopotentials without semicore states. Experimental values (EXP) are from Refs. 29 and 30.

compound SeO_2 and on the Se_2 molecule, we found a narrow distribution of lattice parameters/intermolecular distances and formation energies. Therefore, from the point of view of the structure and energetics of adsorption and kinetics, the effect of the pseudopotential can be considered negligible. The hybrid functional calculations for the Se_2 molecule and for the trigonal solid gave formation and binding energies in between revPBE and PBE results. The convergence of the exchange term, as for bulk Mo, required a $3 \times 3 \times 3$ $\mathbf{q}$-points grid.

Surface calculations have been performed with slabs containing between 5 and 11 layers of Mo and 1 nm of vacuum. The convergence of surface energies was checked versus the number of atomic planes in the slab; the results for up to 11 planes are shown in Table I for the (100) surface, for which the convergence is the slowest. The results presented in the following are for the 7-layer slab, with the exception of the hybrid calculations, for which we used only 5 layers; however, we stress that the same conclusions, for all functionals and adsorption configurations, could have been drawn from the results of the 5-layer slab. Furthermore, the quantitative differences between 5- and 7-layer results are very small, which shows that 5-layer slabs are suitable for studying more complex adsorption superstructures in the future. The in-plane lattice parameter was always chosen to be the equilibrium bcc Mo bulk lattice parameter obtained with the respective pseudopotential/functional. Atomic positions have been fully relaxed up to threshold forces of 10^{-3} Ry/Bohr. K-point meshes of size $9 \times 9 \times 1$ were used for slabs containing only one surface unit cell. For the adsorption at low coverage we used supercells containing 3×3 surface unit cells, with $3 \times 3 \times 1$ k-point meshes.

The geometry of the Mo(110) surface unit cell and the considered adsorption sites are depicted in Fig. 2.

Adsorption energies (per atom) have been calculated as

$$E_{\mathrm{ads}} = \frac{1}{2n}\left(E^{\alpha,N}_{n\mathrm{Se:Mo(110)}} - \alpha E^{1,N}_{\mathrm{Mo(110)}} - 2n\mu_{\mathrm{Se}}\right), \qquad (1)$$

where $E^{\alpha,N}_{n\mathrm{Se:Mo(110)}}$ is the energy calculated for a slab of N planes and α surface unit cells of Mo, with n adsorbed Se atoms on each side of the slab. μ_{Se} and μ_{Mo} are the chemical

TABLE I. Convergence of (100) surface energies as a function of the slab size. Pseudo 1 contains only $4d$ and $5s$ valence states, while pseudo 2 contains also $4s$ and $4p$ semicore states.

		$E_\sigma^{(100)}$ (eV/atom)		E_σ^{100} (J/m^2)	
Functional	No. of planes	Pseudo 1	Pseudo 2	Pseudo 1	Pseudo 2
Q2D-GGA	5	2.646	2.460	4.391	3.995
	7	2.588	2.401	4.295	3.901
	9	2.591	2.396	4.300	3.893
	11	2.570	2.372	4.265	3.854
PBE	5	2.176	1.974	3.512	3.127
	7	2.108	1.909	3.403	3.024
	9	2.091	1.886	3.376	2.987
	11	2.057	1.859	3.320	2.944

potentials for the two elements. For Mo the reference is the bcc metal and for Se we used the trigonal solid, unless specified otherwise. The surface energy, using the slab without Se, is $E_\sigma^{110} = \frac{1}{2}(E^{1,N}_{\mathrm{Mo}(110)} - N\mu_{\mathrm{Mo}})$; analogous formulas hold for other surface orientations. Using the definition of the surface energy, expression (1) can also be written as

$$E_{\mathrm{ads}} = \frac{1}{2n}\left(E^{\alpha,N}_{n\mathrm{Se:Mo}(110)} - 2\alpha E_\sigma^{110} - N\mu_{\mathrm{Mo}} - 2n\mu_{\mathrm{Se}}\right). \qquad (2)$$

III. RESULTS

A. Surface energies

We calculated surface energies for the three high-symmetry surface orientations. Two preliminary comments can be made. As far as the relative stability of the three orientations is concerned, our results are, for all tested functionals, in agreement with previous calculations,[14,31] giving $E_\sigma^{110} < E_\sigma^{111} < E_\sigma^{100}$. At the same time, surface energy values show a non-negligible dependence on the chosen functional and on the inclusion of semicore states in the pseudopotential valence manifold.

The (100) surface—the less stable one according to calculations—is unreconstructed at room temperature, but has been observed to be reconstructed at 100 K.[32,33] The structure was initially thought to be incommensurate,[32] but it was later recognized as a $c(7\sqrt{2} \times \sqrt{2}R45^\circ)$ reconstruction.[33] The expected energy difference at zero temperature between the reconstructed and the unreconstructed surface has been estimated to be quite small, on the order of 0.05 J/m^2, according to a tight-binding calculation.[34] This result justifies our comparison between experimental data and calculations performed for the unreconstructed surface.

The clean (111) surface of molybdenum, less studied than the (100) and (110), is unreconstructed.[35] We did not find any experimental determination of its surface energy.

The surface orientation that is expected to have the lowest surface energy is the (110), according to our calculations and in agreement with previous first-principles estimates.[14,31] However, this expectation is somewhat at variance with available experimental results, for which the (110) and (100) surfaces have very similar surface energies: The only experimental result for the (100), 2.93 J/m^2 (cited in Ref. 14), is only slightly higher than the lowest of the two values reported for the (110) surface, 2.907 and 3.0 J/m^2 (Refs. 14, 31 and 36).

Our results for the surface energies of the three crystal orientations are plotted in panels (a)–(c) of Fig. 3.

In the case of molybdenum, as for copper,[19] the Q2D-GGA functional does not seem to improve the calculated surface energies. The charge redistribution due to the surface creation in Mo is indeed very similar to the one observed for Cu(111),[19] with broad oscillations, as can be seen in Fig. 4.

The inclusion of $4s$ and $4p$ semicore states in the valence manifold of the pseudopotential has a non-negligible effect on the surface energies, which are lowered. Although a higher kinetic-energy cutoff (40 Ryd) slightly reduces this difference, the effect is still clearly present.

The role of semicore states in the bonding of molybdenum was only occasionally mentioned in previous works based

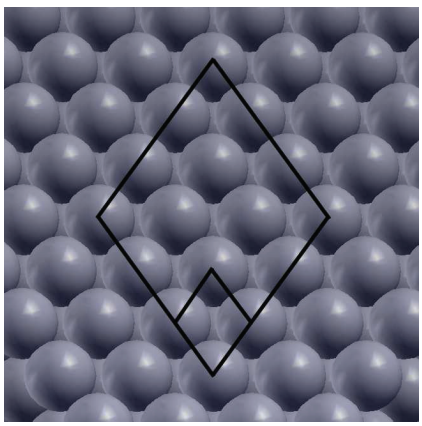

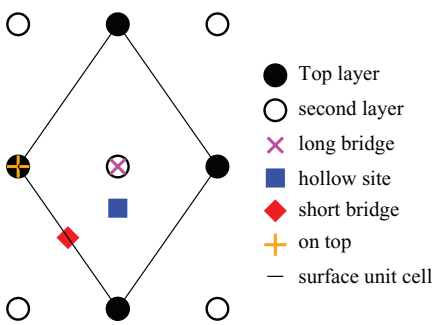

FIG. 2. (Color online) Top view (left panel) of the (110) surface of molybdenum with a sketch of the surface unit cell and the 3×3 surface supercell used for low coverage calculations. The four considered adsorption sites are depicted in the right panel, where the surface unit cell is sketched.

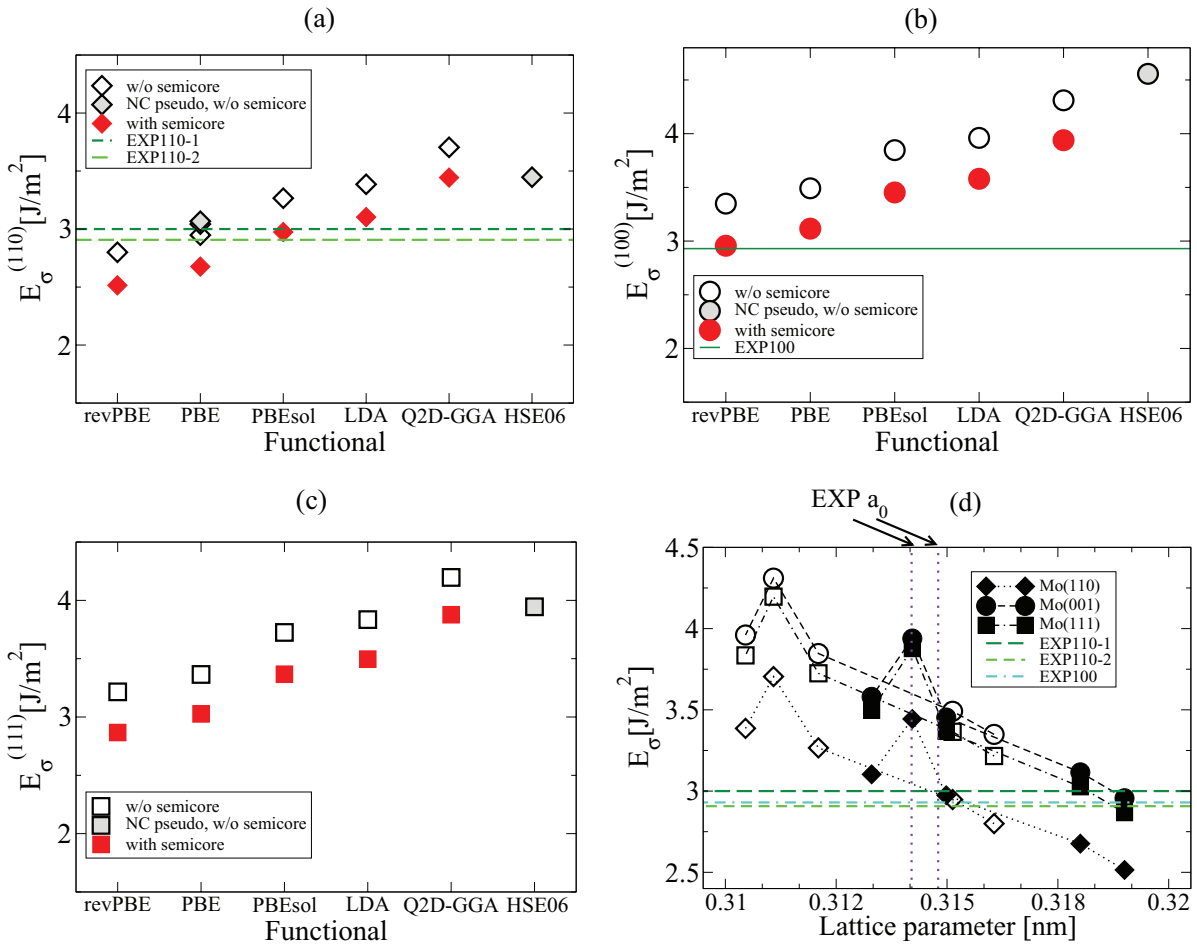

FIG. 3. (Color online) Surface energies of molybdenum for three surface orientations: (110) (a), (100) (b), (111) (c) and for six different xc functionals. Experimental values are from Refs. 36 (EXP110-1), 31 (EXP110-2), and 37 (EXP100). Solid symbols denote results for pseudopotentials with semicore states, open ones denote results for pseudopotentials without them. The gray shaded points were obtained with a norm-conserving pseudopotential without semicore states (NC pseudo). For the sake of comparison we show in panel (a), for the PBE case, results from norm-conserving and ultrasoft pseudopotentials without semicore states (five- and seven-layer data are reported, but are indistinguishable); as expected, the influence of the pseudopotential is small. The fourth panel (d) summarizes the results for surface energies for the semilocal functionals, showing them as a function of the equilibrium lattice parameter of the respective pseudopotential/functional. For each symbol in this panel the functionals are, from left to right, LDA, Q2D-GGA, PBEsol, PBE, revPBE; the connecting dashed/dotted lines are guides for the eye. The dotted vertical lines represent two experimental lattice parameters, from Refs. 29 and 30.

on pseudopotentials. The importance of $4p$ states,[29] and in particular of $4p$-$4p$ hybridization,[38] has been invoked for the description of part of the phonon spectrum of bulk molybdenum, but more recent work is putting this contribution in doubt.[39] We are not aware of works discussing the role of these semicore states for surface properties.

In order to understand the origin of the semicore effect on surface energies, we investigated various aspects. The relaxation of the outermost plane along the z direction, perpendicular to the surface, is very similar in the two cases: If we take the PBE functional, it amounts to -5.52% and -5.02% of the bulk distance, with and without semicore states, respectively. For the slab with only five planes the difference is even smaller (-5.19% vs -5.17%); however, the charge density, as shown in Fig. 4, is clearly different.

We also investigated whether the difference relied on cohesive energies, as there is a relationship between the two quantities.[40] However, the differences in cohesive energies are so small (0.07 eV for PBE and even smaller for LDA and revPBE) that they can account only for a very small part of the difference in surface energies. All these pieces of information suggest that the semicore states are indeed directly involved in surface bonding, at variance with what happens in the bulk.

The surface energies are lowest, for both electronic configurations of pseudopotentials, with the revPBE functional, which also provides the largest lattice parameters. We observe a linear trend between surface energies and lattice parameters which is shown in the fourth panel (d) of Fig. 3. The trend is followed by all semilocal pseudopotentials and functionals except Q2D-GGA, as was previously obtained for other noble and transition metal surfaces,[19] due to the qualitative difference in the description of bidimensional systems with this functional and all the others considered in this work.

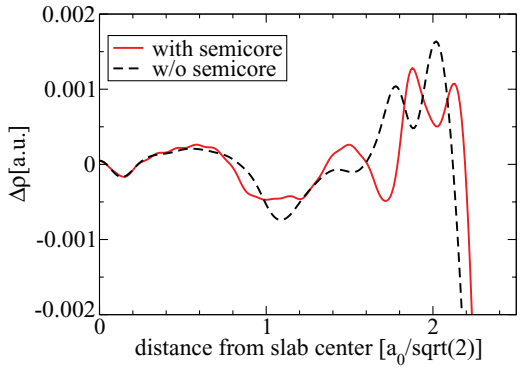

FIG. 4. (Color online) The xy-averaged difference $[\Delta\rho(z)]$ between the surface and the bulk valence charge density for Mo pseudopotentials with and without semicore ($4s$, $4p$) states. Here the xc functional is PBE and the number of planes in the slab is five. The abscissa is in units of the distance between planes in the perfect bulk. Although the structural relaxation is almost identical in the two cases, the $\Delta\rho$ shows notable differences. The oscillations are relatively broad as in the case of Cu (Ref. 19).

Concerning the calculation with the hybrid functional, we find a clear *overestimation* of the surface energies; in fact, it is the worst choice for the (100) surface. This is at variance with the cases of the (111) surfaces of platinum and rhodium,[18] for which the HSE06 functional underestimates the surface energy. This discrepancy can be only partly related to the choice of the pseudopotential; indeed, as shown in the first panel of Fig. 3, the difference between the PBE calculation with the ultrasoft pseudopotential and the one with the norm-conserving pseudopotential used for the hybrid calculation (shaded symbol) is relatively small. From the same figure it is clear that the number of planes in the slab has a negligible influence on the surface-energy value.

B. Adsorption at high coverage

Adsorption of selenium on molybdenum was addressed in early studies devoted to the influence of adsorbed impurities on field emission from metals;[4] i.e., on the induced variation of the work function. However, no clear information on the morphology of the adsorbed film at submonolayer and ML coverage was inferred from those studies. We started, hence, by investigating full ML coverage, although it is not clear from experiments whether this can be achieved before the formation of terraces or reconstructions.

We calculated the adsorption energy for a single ML of selenium on Mo(110) (one Se atom per surface unit cell). Four adsorption sites are possible, for symmetry reasons, on the (110) surface of bcc metals. They are depicted in Fig. 2, right panel.

The pseudopotentials and xc functionals are the same ones that we used for surface energies. The results are shown in the panels of Fig. 5.

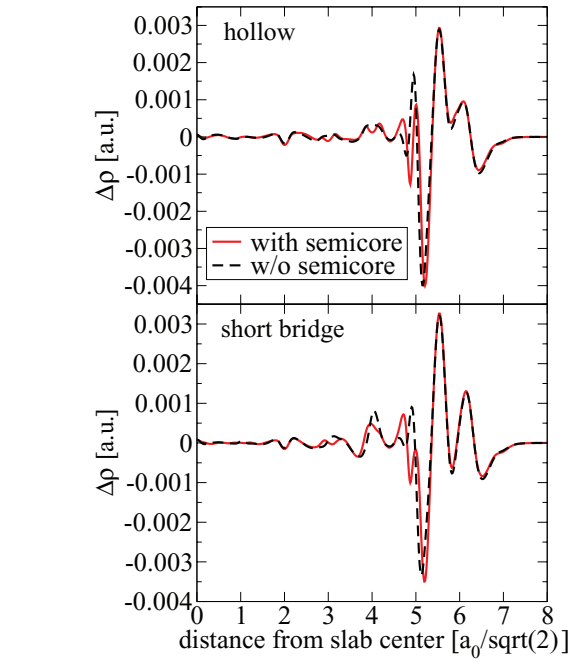

FIG. 6. (Color online) The equivalent of the $\Delta\rho(z)$ shown in Fig. 4 in the case where one ML of Se is present on the surface. The charge that can be attributed to the Se layer is not affected by the semicore states ($4s$ and $4p$) of molybdenum, at variance with the charge at the clean surface. The functional is here Q2D-GGA. There is no significant change in the charge density by varying the xc functional.

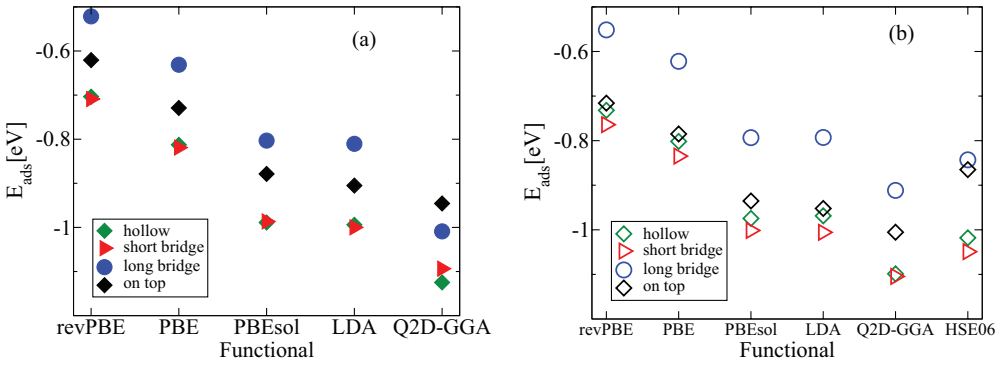

FIG. 5. (Color online) Adsorption energies, in eV per adsorbed atom, for the LDA, four semilocal xc functionals, and HSE06. On the left (a), the pseudopotential for Mo additionally includes $4s$ and $4p$ states in the valence manifold; on the right (b), only $4d$ and $5s$ are considered as valence states. The reference state for selenium is the trigonal solid ground state.

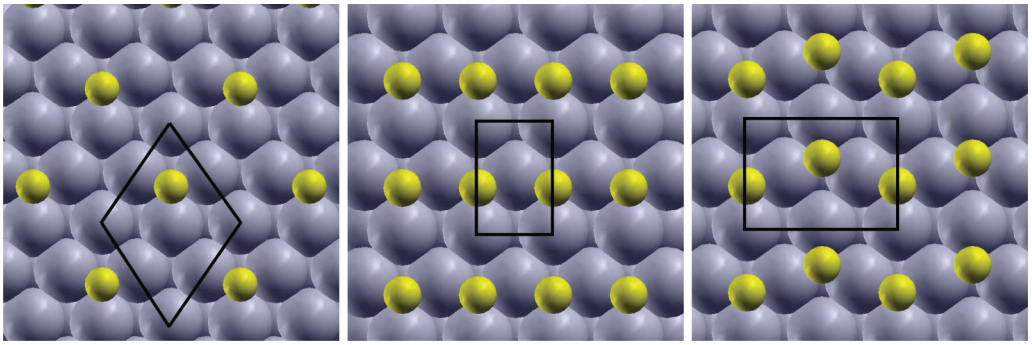

FIG. 7. (Color online) Three surface adsorption structures on the Mo(110) surface, usually referred to as (from left to right) $p(2 \times 2)$, $c(2 \times 2)$, and $\left[\begin{smallmatrix} 2 & \bar{2} \\ 1 & 1 \end{smallmatrix}\right]$. The coverage is $\theta = 0.25$ for the first one, $\theta = 0.50$ for the others. Surface unit cells are sketched in black. The adsorption energetics for these structures are discussed in the text for S and Se.

The data suggest two remarks. The first is that, as discussed by Schimka and co-workers,[18] the trend for adsorption energy vs functional is reversed with respect to that observed for surface energies: The adsorption energy lowers (i.e., becomes more negative, or the adsorbate is more stable) when going from revPBE to Q2D-GGA, while surface energies grow. Here the HSE06 functional gives results close to the LDA or PBEsol, with a notable exception in the relative stability of the on top and long bridge sites, which are very close in energy.

The second remark is related to the effect of the inclusion of semicore states, which is less crucial for adsorption energies than for surface energies. The difference between adsorption energies at the same site does not exceed 0.1 eV per adsorbed atom, whereas the surface energy can vary by as much as 0.5 eV per surface atom when semicore states are included. The fact that the presence of semicore states tends to raise the adsorption energy while lowering the surface energy is an indication that those states are more involved in the metallic bonding of Mo at the surface than in the Mo-Se bonding, as can be inferred from Eq. (2). Inspection of the charge distribution (Fig. 6) confirms that semicore states have little influence on the Mo-Se bonding, as the shape of the Se charge at the surface is nearly unaffected by the change in the pseudopotential.

The most stable adsorption site is the short bridge for both types of pseudopotentials and for all functionals except the Q2D-GGA. The short bridge is followed, as stability is concerned, by the hollow, the on top, and the long bridge sites. The Q2D-GGA and the HSE06 are the only functionals showing a slightly different relative stability of adsorption sites, with the on top and long bridge closer in energy. The short bridge and hollow sites are also predicted to be very close in energy. The Q2D-GGA is the only functional for which the long bridge site is an unstable configuration (only when semicore states are included), relaxing to an intermediate geometry between long bridge and hollow.

The predictive power of the Q2D-GGA functional is clearly reduced in the case of the Mo clean surface, as we previously mentioned, due to relatively wide spread surface charge oscillations. However, for the adsorbed Se ML, the surface charge is more two-dimensional in character, with large and narrow charge oscillations as seen on Pt or Au clean surfaces,[19] for which Q2D-GGA gives the best results. An experimental investigation of the structure and energetics of Se adsorbed on the (110) surface of Mo is unfortunately not available; such a study would allow us to determine whether the Q2D-GGA functional gives better predictions than the other tested approximations in this system.

C. A comparison with sulfur adsorption at submonolayer coverages

Due to the lack of experimental and theoretical information on the adsorption of Se on Mo surfaces, we can establish a comparison with the adsorption of the chemically similar group VI element sulfur, for which experimental and first-principles[8,9] studies have been performed. Two adsorption patterns have been observed, corresponding to coverages of 0.25 and 0.50 ML of S on Mo(110). These two structures, plus a third one discussed for S, are shown in Fig. 7. According to the calculations of Chen and coworkers,[8] the observed pattern for the 0.50 ML coverage corresponds to a $\left[\begin{smallmatrix} 2 & \bar{2} \\ 1 & 1 \end{smallmatrix}\right]$ symmetry, more stable than the $c(2 \times 2)$ by 0.31 eV, with S atoms always in the hollow site. The picture for Se, as predicted by our calculations, is qualitatively similar, with the zigzag selenium chains of the $\left[\begin{smallmatrix} 2 & \bar{2} \\ 1 & 1 \end{smallmatrix}\right]$ structure favored by $\Delta E_{\text{ads}} = 0.08$ eV per adsorbed atom with respect to the $c(2 \times 2)$ symmetry.

TABLE II. Comparison of Se vs S binding energies on Mo(110) at two different coverages (θ), corresponding to two adsorption structures. Energies are in eV per adsorbed atom. Data for sulfur in the first two columns are from Refs. 8 and 9.

Structure	S, Ref. 8 (LDA)	S, Ref. 9 (PBE)	S (PBE)	S (LDA)	Se (PBE)	Se (LDA)
$p(2 \times 2)$ $\theta = 0.25$ ML		−6.50	−6.41	−7.54	−5.84	−6.85
$c(2 \times 2)$ $\theta = 0.50$ ML	−5.77	−6.14	−5.78	−6.89	−5.14	−6.14
$\left[\begin{smallmatrix} 2 & \bar{2} \\ 1 & 1 \end{smallmatrix}\right]$ $\theta = 0.50$ ML	−6.08		−5.91	−7.00	−5.28	−6.28

TABLE III. Adsorption energies for Se on Mo(110) taking as a reference trigonal selenium. We show the same three structures as in Table II, corresponding to two coverages (θ). We compare LDA, PBE, and Q2D-GGA functionals. In parentheses we show results for the Mo pseudopotential without semicore states.

Structure	PBE	LDA	Q2D-GGA
$p(2\times 2)$ $\theta = 0.25$ ML	−3.25 (−3.41)	−3.37 (−3.55)	−3.27 (−3.45)
$c(2\times 2)$ $\theta = 0.50$ ML	−2.55 (−2.67)	−2.66 (−2.79)	−2.68 (−2.81)
$\begin{bmatrix} 2 & \bar{2} \\ 1 & 1 \end{bmatrix}$ $\theta = 0.50$ ML	−2.69 (−2.83)	−2.80 (−2.94)	−2.80 (−2.94)

However, in the latter case, the Se atoms relax towards the long bridge position (although slightly displaced from it by 0.11 Å), while in the $\begin{bmatrix} 2 & \bar{2} \\ 1 & 1 \end{bmatrix}$ structure, they form a zigzag chain residing on hollow sites, as for sulfur. Even if the structural relaxation is performed starting with Se atoms on short bridge sites, the most stable structure turns out to be the one with Se in hollow sites.

Both the cited DFT studies[8,9] of S:Mo(110) provide, for the calculated adsorption structures, the sulfur binding energies to the surface (i.e., adsorption energies with reference to an isolated atom). We compare in Table II their results for sulfur adsorption with those obtained here for selenium, using the PBE and LDA functionals and the pseudopotential with semicore states. The omission of semicore states in the pseudopotential has a very weak effect as far as the energy difference between adsorption patterns is concerned (0.1 eV vs 0.08 eV for ΔE_{ads}) and changes the absolute value of the adsorption energies by approximately 0.1 eV. The use of LDA, or even more so the use of Q2D-GGA, further reduces the ΔE_{ads} to approximately 0.05 eV. For comparison and for the sake of completeness, we also calculated the three structures for sulfur; the results are shown in Table II.

The binding energies that we calculated with LDA (and even more so with Q2D-GGA) have a larger magnitude than those calculated using PBE, when considering a single atom as a reference state. The difference of around 1 eV for both sulfur and selenium is not surprising, given the known tendency of the LDA to overbind, a tendency which is corrected by the GGA. However, a comparison of the LDA results of Chen and co-workers[8] with those of Zhou and co-workers,[9] obtained with PBE, shows the opposite, at least in the case of the $c(2\times 2)$ structure. Although we do not know the details of the pseudopotentials used in the two cited works, we can speculate that the difference between the two results has to be ascribed more to the pseudopotentials than to the xc functional, because the total energy of an isolated atom, i.e., the reference energy, depends, of course, on the electronic configuration used for the pseudopotential generation.

If one takes trigonal solid selenium as a reference, a physically more sensible choice than the isolated atom, the calculated adsorption energies are very weakly affected by the choice of the xc functional, as can be inferred from the data that we present in Table III. The relative stability of the three adsorption structures is independent of the functional and of the pseudopotential set.

TABLE IV. Adsorption energies (in eV/Se) of Se on Mo(110) at low coverage ($\theta = 0.11$): comparison of two pseudopotential sets, with the PBE functional. Pseudo set 2 includes semicore states $4s$ and $4p$ in the valence, while pseudo set 1 has only $4d$ and $5s$ states in valence.

Adsorption site	Pseudo set 1	Pseudo set 2
Hollow	−3.03	−2.81
Short bridge	−2.56	−2.37
Long bridge	−3.07	−2.86
On top	−1.53	−1.40

D. Adsorption at low coverage

In order to predict the adsorption energy for an isolated Se atom on the Mo(110) surface, we used the supercell described in Sec. II, corresponding to a coverage $\theta = 0.11$. We tested the four possible adsorption sites, as we did for full coverage, within LDA, PBE, and Q2D-GGA functionals. The hollow site relaxes, at low coverage, to a position that is only very slightly displaced along the y direction with respect to the long bridge site (L); the latter was the least stable one at high coverage. The y displacement between the relaxed hollow site and the long bridge position varies between 0.06 and 0.24 Å, depending on the functional and the pseudopotential. The energies of the long bridge and the relaxed hollow site are identical within the precision of the calculation, so that we can consider the intermediate position to be a single unique site, which turns out to be the most stable one at this coverage.

A comparison among the three considered functionals is shown in Fig. 8: Here the effect of the functional is weaker

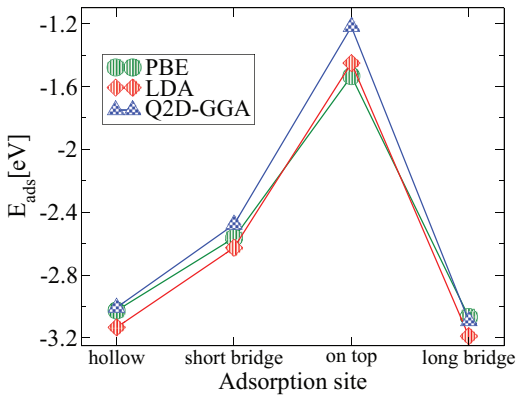

FIG. 8. (Color online) Adsorption energies for Se on Mo(110) at low coverage ($\theta = 0.11$) for PBE, LDA, and Q2D-GGA functional. The most stable adsorption site at low coverage, the *long bridge*, is the least stable one at full coverage ($\theta = 1$, see Fig. 5).

than at high coverage for the most stable adsorption site, but is slightly stronger for the less stable one. Thus, the xc functional seems to have a somewhat stronger influence on energy differences between adsorption sites than on the most stable state. In any case, the on top site is much higher in energy than the long bridge/hollow site—the most stable one—or the short bridge site.

IV. CONCLUSIONS

In this work we have reported results of first-principles calculations of surface energies for the three high-symmetry crystal orientations, as well as calculations of Se adsorption on the Mo(110) surface at various coverages.

We have investigated in some detail the effect of some common approximations, namely, the choice of the xc functional and the inclusion or not of semicore states in the valence manifold of the molybdenum pseudopotential. Concerning the xc functional, we have tested some common functionals (local, semilocal, and hybrid), including the recently proposed Q2D-GGA, which is known to improve the surface-energy description of many transition metals.

As a first conclusion, all tested functionals tend to overestimate the Mo(100) surface energy. In particular, surface energies of molybdenum, like those of copper, are overestimated by the Q2D-GGA functional, due to the charge density rearrangement at the surface, as well as by the HSE06 hybrid functional. These surfaces do not show a very strong quasi-two-dimensional character of the electronic charge at the material/vacuum interface; thus, a better choice for these systems seems to be PBE or PBEsol, which give results in agreement with experiment for the (110) surface. Concerning the (100) surface, further theoretical and experimental investigations are necessary to clarify whether the origin of the overestimation may be found in the reconstruction energy, in a specific failure of tested functionals, or in the reliability of the sole available experimental figure.

As far as adsorption energetics is concerned, a comparison with the case of sulfur shows that Se:Mo(110) has somewhat higher adsorption energies (i.e., smaller binding energies); this could be expected from the position on the periodic table, suggesting that $E_{\mathrm{ads}}(\mathrm{O}) < E_{\mathrm{ads}}(\mathrm{S}) < E_{\mathrm{ads}}(\mathrm{Se})$. The relative stability of three adsorption structures at intermediate coverage is similar to the case of sulfur, with a preferred pattern at $\theta = 0.5$ ML consisting of zigzag chains of Se atoms sitting in *hollow* positions. Conversely, at 1 ML coverage, the most stable adsorption site turns out to be the *short bridge*, for all functionals except Q2D-GGA.

At low coverage the influence of the xc functional is weak for the most stable adsorption site, which is an intermediate position between the hollow and long bridge sites. For the less stable site, the on top one, the energy difference between functionals is somewhat larger. The hierarchy of stability of different adsorption sites is independent of functionals and of pseudopotentials.

ACKNOWLEDGMENTS

G.R. acknowledges financial support from the Advanced Materials CEA-DEN program (MATAV) and from the Federal Ministry for the Environment, Nature Conservation, and Nuclear Safety, based on a decision of the Parliament of the Federal Republic of Germany, under the comCIGS II project. This work was performed using mainly HPC resources from GENCI-CCRT (Grant No. 2012-gen6018). We are grateful to Erin Hayward for a careful reading of the manuscript.

*Present address: Center for Life Nano Science @Sapienza, Istituto Italiano di Tecnologia, Viale Regina Elena 291, I-00161, Roma, Italy.

[1] K. Ramanathan, M. A. Contreras, C. L. Perkins, S. Asher, F. S. Hasoon, J. Keane, D. Young, M. Romero, W. Metzger, R. Noufi, J. Ward, and A. Duda, Prog. Photovoltaics **11**, 225 (2003).

[2] P. Jackson, D. Hariskos, E. Lotter, S. Paetel, R. Wuerz, R. Menner, W. Wischmann, and M. Powalla, Prog. Photovoltaics **19**, 894 (2011).

[3] R. Caballero, C. A. Kaufmann, T. Eisenbarth, A. Grimm, I. Lauermann, T. Unold, R. Klenk, and H. W. Schock, Appl. Phys. Lett. **96**, 092104 (2010).

[4] R. Collins and C. Kiwanga, Surf. Sci. **61**, 491 (1976).

[5] D. Abou-Ras, G. Kostorz, D. Bremaud, M. Kälin, F. V. Kurdesau, A. N. Tiwari, and M. Döbeli, Thin Solid Films **480-481**, 433 (2005).

[6] S. Ahn, K. Kim, and K. Yoon, in *IEEE 4th World Conference on Photovoltaic Energy Conversion* (IEEE, Piscataway, NJ, 2006), Vol. 1, pp. 506–508.

[7] R. Krishnan, E. Payzant, R. Kacnyzki, U. Schoop, J. Britt, R. Noufi, and T. Anderson, in *35th IEEE Photovoltaic Specialists Conference* (IEEE, Piscataway, NJ, 2010), pp. 001006–001008.

[8] M. Chen, P. G. Clark, T. Mueller, C. M. Friend, and E. Kaxiras, Phys. Rev. B **60**, 11783 (1999).

[9] Y. G. Zhou, X. T. Zu, J. L. Nie, and H. Y. Xiao, Chem. Phys. **353**, 109 (2008).

[10] D. Proskurin, A. Nikolaychik, I. F. Koval, and I. N. Yakovkin, Phys. Status Solidi B **243**, 584 (2006).

[11] D. Wu, W. K. Lau, Z. Q. He, Y. J. Feng, M. S. Altman, and C. T. Chan, Phys. Rev. B **62**, 8366 (2000).

[12] K. Kośmider, A. Krupski, P. Jelínek, and L. Jurczyszyn, Phys. Rev. B **80**, 115424 (2009).

[13] Y. Zhou, X. Zu, J. Nie, and F. Gao, Eur. Phys. J. B **67**, 27 (2009).

[14] J. G. Che, C. T. Chan, W.-E. Jian, and T. C. Leung, Phys. Rev. B **57**, 1875 (1998).

[15] B. Kohler, P. Ruggerone, S. Wilke, and M. Scheffler, Phys. Rev. Lett. **74**, 1387 (1995).

[16] T. Schlenker, V. Laptev, H. Schock, and J. Werner, Thin Solid Films **480-481**, 29 (2005).

[17] P. Giannozzi *et al.*, J. Phys.: Condens. Matter **21**, 395502 (2009).

[18] L. Schimka, J. Harl, A. Stroppa, A. Grüneis, M. Marsman, F. Mittendorfer, and G. Kresse, Nat. Mater. **9**, 741 (2010).

[19] L. Chiodo, L. A. Constantin, E. Fabiano, and F. Della Sala, Phys. Rev. Lett. **108**, 126402 (2012).

[20] See Supplemental Material at http://link.aps.org/supplemental/10.1103/PhysRevB.87.245420 for all pseudopotential files.

[21] W. Kohn and L. J. Sham, Phys. Rev. **140**, A1133 (1965).

[22] J. P. Perdew, K. Burke, and M. Ernzerhof, Phys. Rev. Lett. **77**, 3865 (1996).

[23]J. P. Perdew, A. Ruzsinszky, G. I. Csonka, L. A. Constantin, and J. Sun, Phys. Rev. Lett. **103**, 026403 (2009).
[24]Y. Zhang and W. Yang, Phys. Rev. Lett. **80**, 890 (1998).
[25]J. Heyd, G. E. Scuseria, and M. Ernzerhof, J. Chem. Phys. **118**, 8207 (2003).
[26]A. V. Krukau, O. A. Vydrov, A. F. Izmaylov, and G. E. Scuseria, J. Chem. Phys. **125**, 224106 (2006).
[27]M. Fuchs and M. Scheffler, Comput. Phys. Commun. **119**, 67 (1999).
[28]F. Gygi and A. Baldereschi, Phys. Rev. B **34**, 4405 (1986).
[29]D. Singh and H. Krakauer, Phys. Rev. B **43**, 1441 (1991).
[30]Y. Zhao, A. C. Lawson, J. Zhang, B. I. Bennett, and R. B. Von Dreele, Phys. Rev. B **62**, 8766 (2000).
[31]L. Vitos, A. Ruban, H. Skriver, and J. Kollár, Surf. Sci. **411**, 186 (1998).
[32]T. E. Felter, R. A. Barker, and P. J. Estrup, Phys. Rev. Lett. **38**, 1138 (1977).
[33]E. Hulpke and D.-M. Smilgies, Phys. Rev. B **43**, 1260 (1991).
[34]H. Haas, C. Z. Wang, K. M. Ho, M. Fähnle, and C. Elsässer, Surf. Sci. Lett. **457**, L397 (2000).
[35]I. N. Yakovkin, M. Kuchowicz, R. Szukiewicz, and J. Kołaczkiewicz, Surf. Sci. Lett. **600**, 240 (2006).
[36]W. Tyson and W. Miller, Surf. Sci. **62**, 267 (1977).
[37]A. R. Miedema, Z. Metallkd. **69**, 287 (1978), cited in Ref. 14.
[38]S. Buck, K. Hummler, and M. Fähnle, Phys. Status Solidi B **195**, K9 (1996).
[39]D. L. Farber, M. Krisch, D. Antonangeli, A. Beraud, J. Badro, F. Occelli, and D. Orlikowski, Phys. Rev. Lett. **96**, 115502 (2006).
[40]M. Methfessel, D. Hennig, and M. Scheffler, Phys. Rev. B **46**, 4816 (1992).